

# Positive-Negative Birefringence in Multiferroic Layered Metasurfaces

R. Khomeriki

*Institut für Physik, Martin-Luther-Universität, Halle-Wittenberg, D-06099 Halle/Saale, Germany  
Physics Department, Tbilisi State University, 3 Chavchavadze, 0128 Tbilisi, Georgia*

L. Chotorlishvili

*Institut für Physik, Martin-Luther-Universität, Halle-Wittenberg, D-06099 Halle/Saale, Germany*

I. Tralle

*Faculty of Mathematics and Natural Sciences, University of Rzeszow, Pigońia 1, 35-310 Rzeszow, Poland*

J. Berakdar

*Institut für Physik, Martin-Luther-Universität, Halle-Wittenberg, 06099 Halle/Saale, Germany\**

We uncover and identify the regime for a magnetically and ferroelectrically controllable negative refraction of light traversing multiferroic, oxide-based metastructure consisting of alternating nanoscopic ferroelectric (SrTiO<sub>2</sub>) and ferromagnetic (Y<sub>3</sub>Fe<sub>2</sub>(FeO<sub>4</sub>)<sub>3</sub>, YIG) layers. We perform analytical and numerical simulations based on discretized, coupled equations for the self-consistent Maxwell/ferroelectric/ferromagnetic dynamics and obtain a biquadratic relation for the refractive index. Various scenarios of ordinary and negative refraction in different frequency ranges are analyzed and quantified by simple analytical formula that are confirmed by full-fledge numerical simulations. Electromagnetic-waves injected at the edges of the sample are propagated exactly numerically. We discovered that for particular GHz frequencies, waves with different polarizations are characterized by different signs of the refractive index giving rise to novel types of phenomena such as a positive-negative birefringence effect, and magnetically controlled light trapping and accelerations.

## INTRODUCTION

According to Veselago's predictions [1, 2] that were later confirmed experimentally [3–5], negative refraction phenomena occur in metamaterials where both the electric permittivity  $\epsilon$  and the magnetic permeability  $\mu$  are negative. The Poynting and the wave vectors are then antiparallel resulting in a phase decrease during the propagation process. A clear example of this phenomena is based on metallic heterostructures [6] which are inherently absorptive at relevant frequencies [7]. To avoid losses, insulating multiferroics may offer a solution [8, 9], but also new possibilities for external control and exploitations of functional materials. Multiferroics are one-phase or composite, synthesized structures exhibiting simultaneously multiple orderings such as ferromagnetic, ferro and/or piezoelectric order and respond thus to a multitude of conjugate fields. This class of materials plays a key role for addressing fundamental issues regarding the interplay between electronic correlation, symmetry, magnetism, and polarization. Potential applications are diverse, ranging from sensorics and magnetoelectric spintronics to environmentally friendly devices with ultralow energy consumption [10, 11].

Here, we demonstrate how multiferroics properties lead to exotic electromagnetic wave propagation features. In particular, we demonstrate the existence of a negative refraction in ferroelectric (FE)/ferromagnetic(FM) multilayers. The large (FE and FM) resonance frequency mismatch between ferroelectric and ferromagnetic media

is usually an obstacle. Indeed, the paradigm ferroelectric BaTiO<sub>3</sub> has a resonance frequency in THz range [12–15], while the insulating ferromagnet, rhodium-substituted  $\epsilon$ -Rh<sub>x</sub>Fe<sub>2-x</sub>O<sub>3</sub> with largest known coercivity has characteristic frequencies in 200GHz range [16]. On the other hand, ferroelectric SrTiO<sub>2</sub> (STO) [17] does possess overlapping resonances with the well-investigated insulating ferromagnet Y<sub>3</sub>Fe<sub>2</sub>(FeO<sub>4</sub>)<sub>3</sub> (also called YIG) [18]. A number of further insulating FE, and FM insulating oxides are also possible, for concreteness we present and discuss here the results for STO/YIG/STO/... structures. In the pilot numerical simulations below we choose the FE layer to be 10 nm and the FM layer to be 1  $\mu$ m. As we will be working in reduced units, meaning the effects are scalable; for materials composites responding at higher frequencies, smaller structures are appropriate.

In earlier studies the negative refraction effect was observed in specific systems embracing two different subparts with  $\epsilon < 0$ ,  $\mu > 0$ , and  $\epsilon > 0$ ,  $\mu < 0$  respectively [8, 9]. We note that in the same medium propagating positively refracting mode can exist as well [9]. In the present paper, we study the FE/FM composite (cf. the schematics setup in Fig. 1a) with an eye to find the frequency domain where both negatively and positively refracting waves with different polarizations simultaneously coexist for the same excitation frequency. By this we predict that in the suggested system unpolarized electromagnetic wave undergoes both positive and negative refractions, manifesting a novel positive-negative birefringence effect.

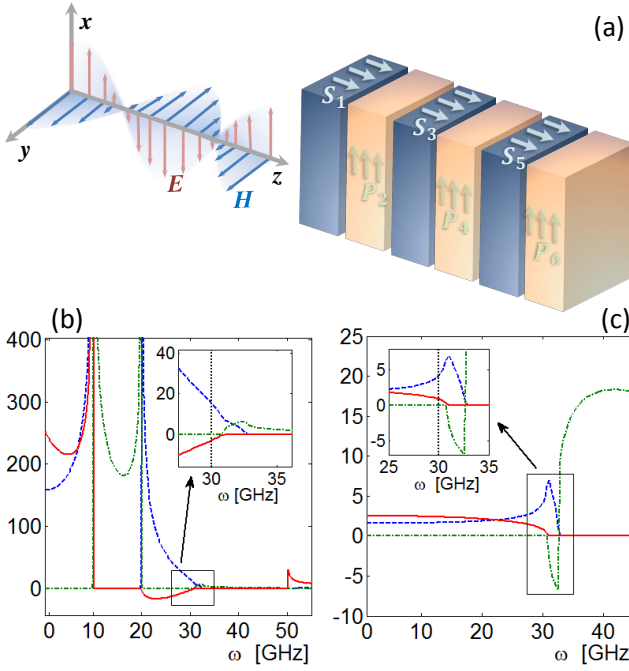


FIG. 1: (a) Schematics for the photonic/ferroelectric/ferromagnetic heterostructure. The electric polarization  $\mathbf{P}_j$  in the layer  $j$  is aligned along  $x$  axis. The incident light wave propagating along  $z$  axis.  $\mathbf{E}$  and  $\mathbf{H}$  denote the electric and magnetic field components. The magnetization  $\mathbf{S}_i$  in the layer  $i$  points also along the  $z$  axis. (b) and (c) graphs show real (dashed blue curve) and imaginary (dashed-dotted green curve) parts of the refractive index  $n$  versus the mode frequency according to the biquadratic equation (5). Red solid curve is the  $z$  component of the time averaged dimensionless Poynting vector  $\langle W_z \rangle / P_0 S_0$  as calculated by means of the formula (6). Graphs (b) and (c) correspond to the negatively and positively refracting waves, respectively for the same excitation frequency 30GHz indicated by vertical dotted lines in the insets. Insets display enlarged views of the frequencies in interest. The FE/FM specific materials are detailed in the text.

## MODEL AND PARAMETERS

Let both the thickness of the YIG and the STO layers be equal  $a$ , for clarity. We denote the positions of STO and YIG layers by even  $(2m)$  and odd  $(2m-1)$  integer numbers respectively, where  $m = 1, 2, \dots, N/2$ . For the description of light-induced FE/FM dynamics and its backaction on the light propagation properties we will utilize a discretized Maxwell materials equation self-consistently coupled to the FE dynamics as described by the Ginzburg-Landau-Devonshire (GLD) method, and a classical Heisenberg model for the magnetization precession. This low-energy effective treatment is well-justified due to the choice of the appropriate frequency and the (low to moderate) intensity of the incident light wave. The discretized FE polarization  $P_{2m}$  (initially along  $x$  axis) and FM magnetization  $\vec{S}_{2m-1}$  (initially along  $z$

axis) (cf. Fig. 1a) are thus described by the energy functional

$$\mathcal{H} = \mathcal{H}_P + \mathcal{H}_S, \quad \mathcal{H}_P = \sum_{m=1}^{N/2} \left[ \frac{\alpha_0}{2} \left( \frac{dP_{2m}}{dt} \right)^2 - \frac{\alpha_1}{2} (P_{2m})^2 + \frac{\alpha_2}{4} (P_{2m})^4 - P_{2m} E_{2m}^x \right], \quad (1)$$

$$\mathcal{H}_S = - \sum_{m=1}^{N/2} \left[ H_0 S_z + D (S_{2m-1}^z)^2 + \vec{H}_{2m-1} \vec{S}_{2m-1} \right],$$

where  $\alpha_0$  stands for the kinetic constant,  $\alpha_1$  and  $\alpha_2$  are potential coefficients of the FE part, and  $D$  is a uniaxial anisotropy constant in FM layers.  $H_0$  is a static external magnetic field applied along the  $z$  axis which will prove useful for tuning the functional properties of the setup, e.g. for switching between the ordinary and the negative refraction regimes (see below).

We assume that the multilayer structure is first driven to saturation by appropriately strong fields. The remnant FE and FM polarizations are then denoted by  $P_0$  and  $S_0$ . Let us introduce dimensionless photonic field  $\vec{h} \equiv \vec{H}/S_0$ , and  $\vec{\mathcal{E}} \equiv \vec{E}/P_0$  and denote small deviations around the ordering directions by  $p_{2m} \equiv P_0 - P_{2m}$ , and  $\vec{s}_{2m-1} \equiv \vec{S}_0 - \vec{S}_{2m-1}$ . The thickness of the layers (along the propagation direction) should be small enough such that no domains are formed along the  $z$  axis (the general case of large  $a$  is captured also with this model by adding pinning sites and appropriate energy contributions to eq.(1), but this is expected to be subsidiary to the effects discussed here). Our propagating electromagnetic wave cannot create domains since the wavelength far exceeds  $a$ . The discretized form of Maxwell's equations for the electromagnetic field vectors read

$$\begin{aligned} \frac{1}{c} \frac{d}{dt} (h_{2m+1}^x + 4\pi s_{2m+1}^x) &= \frac{1}{2a} (\mathcal{E}_{2m+2}^y - \mathcal{E}_{2m}^y) \\ -\frac{1}{c} \frac{d}{dt} (h_{2m+1}^y + 4\pi s_{2m+1}^y) &= \frac{1}{2a} (\mathcal{E}_{2m+2}^x - \mathcal{E}_{2m}^x) \\ -\frac{1}{c} \frac{d}{dt} (\mathcal{E}_{2m}^x + 4\pi p_{2m}) &= \frac{1}{2a} (h_{2m+1}^y - h_{2m-1}^y) \\ \frac{1}{c} \frac{d}{dt} \mathcal{E}_{2m}^y &= \frac{1}{2a} (h_{2m+1}^x - h_{2m-1}^x). \end{aligned} \quad (2)$$

These equations need to be propagated simultaneously with the dynamics governed by eqs.(1). Nonlinear corrections are irrelevant when the relative values of the polarization and the magnetization of eigenmodes are much smaller than unity. Thus, the validity of the linear approximation can be checked directly by monitoring the relative eigenmodes. After these simplifications, from (1) we infer the linearized, coupled photonic-matter evolu-

tion equations

$$\begin{aligned} \frac{d^2 p_{2m}}{dt^2} &= -\omega_P^2 p_{2m} + \frac{\omega_P^2}{4\pi\alpha} \mathcal{E}_{2m}^x & (3) \\ \frac{\partial s_{2m+1}^x}{\partial t} &= -\omega_0 s_{2m+1}^y + \frac{\omega_M}{4\pi} h_{2m+1}^y \\ \frac{\partial s_{2m+1}^y}{\partial t} &= \omega_0 s_{2m+1}^x - \frac{\omega_M}{4\pi} h_{2m+1}^x. \end{aligned}$$

The FE resonance frequency  $\omega_P$  of STO is around  $\omega_P = 10$  GHz. The GDL potential curvature at equilibrium  $\alpha = 2\alpha_1$  is related to the electric susceptibility at the zero mode frequency as  $\chi(0) = 1/4\pi\alpha$ . For the large permittivity observed in Ref. [17] the potential curvature is of the order of  $\alpha \sim 10^{-4}$ . For YIG [18] the Larmor frequency is  $\omega_0 = \gamma H_0 + 2D\gamma S_0$  (in zero external field  $\omega_0 = 20$ GHz) and  $\omega_M = 4\pi\gamma S_0 = 30$ GHz ( $\gamma$  is the gyromagnetic ratio for electrons).

For a linearly polarized electromagnetic waves in the FE/FM multilayers the refractive index follows from the matter equations (3). The expressions for the permittivity  $\epsilon = 1 + \frac{\omega_P^2/\alpha}{\omega_P^2 - \omega^2}$  and the permeability  $\mu = 1 + \frac{\omega_0\omega_M}{\omega_0^2 - \omega^2}$  for the linearly polarized wave components  $\mathcal{E}_x, h_y$  indicate that

$$n_1^2 = \epsilon\mu = \left(1 + \frac{\omega_P^2/\alpha}{\omega_P^2 - \omega^2}\right) \left(1 + \frac{\omega_0\omega_M}{\omega_0^2 - \omega^2}\right). \quad (4)$$

In spite of the fact that a linearly polarized wave is not an eigenmode of the FE-FM system, the eigenmode (4) has a certain merit. The asymptotic solution corresponds to the large susceptibility limit (see below). In order to precisely calculate the refractive index, one needs to solve a complete set of coupled Maxwell (2) and matter (3) equations. Thus looking for a general solution we proceed further and adopt an ansatz presenting field and matter wave components as follows:  $\mathcal{E}_m^x = \mathcal{E}_x e^{i(\omega t - kam)}$ . Here  $a$  is a FE/FM lattice constant  $\omega$  and  $k$  are the eigenmode frequency and wavenumber, respectively. Analyzing the linear algebraic equations (see Supporting Information for the details) we arrive at the following biquadratic equation for the refractive index  $n \equiv ck/\omega$ .

$$\begin{aligned} &\alpha(\omega_0^2 - \omega^2)(\omega_P^2 - \omega^2)n^4 - & (5) \\ &-(\omega_0^2 + \omega_M\omega_0 - \omega^2) [2\alpha(\omega_P^2 - \omega^2) + \omega_P^2] n^2 + \\ &+ [\alpha(\omega_P^2 - \omega^2) + \omega_P^2] [(\omega_0 + \omega_M)^2 - \omega^2] = 0, \end{aligned}$$

and a set of amplitudes for the field and matter wave components. Then it is straightforward to calculate the time averaged dimensionless Poynting vector  $\mathcal{W} = \langle W_z \rangle / P_0 S_0$  as

$$\begin{aligned} \mathcal{W} &= \langle E_x H_y - E_y H_x \rangle / P_0 S_0 = [\mathcal{E}_x h_y^* - \mathcal{E}_y h_x^*] + c.c. \\ &= n \left\{ \frac{(\omega^2 - \omega_P^2) [(\omega^2 - \omega_0^2)(n^2 - 1) + \omega_0\omega_M]^2}{(\omega^2 - \omega_P^2 - \omega_P^2/\alpha)\omega^2\omega_M^2} + 1 \right\}. & (6) \end{aligned}$$

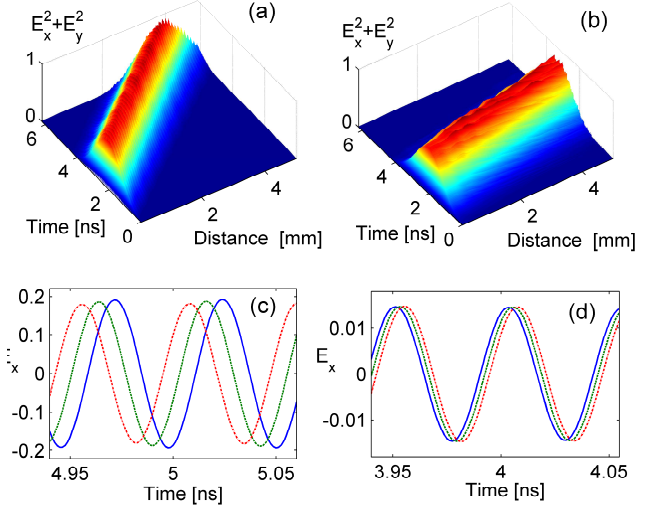


FIG. 2: Graphs (a) and (c) represent negative refraction injecting the signal with a polarization  $\mathcal{E}_{x,y} = 0.19 + 1.81i$ , while Graphs (b) and (d) display positive refraction of the wave with polarization  $\mathcal{E}_{x,y} = 0.015 + 1.985i$  corresponding to a positive refraction. In graphs (c) and (d) blue (solid), green (dashed-dotted) and red (dashed) curves correspond to time oscillations of the FE/FM layers with increasing site numbers.

It is straightforward to derive from (5) the two obvious limiting cases of pure ferromagnet or ferroelectrics. For zero magnetization, we set  $\omega_M = 0$  and from (5) obtain two linearly polarized eigenmodes with the refractive indexes  $n_1 = 1$  and  $n_2 = \sqrt{1 + \frac{\omega_P^2/\alpha}{\omega_P^2 - \omega^2}}$  corresponding to the polarizations along  $y$  and  $x$  axis, respectively. In the case of a vanishing polarization in the system we set  $\alpha \rightarrow \infty$  and find two circularly polarized eigenmodes characterized by different refractive indexes  $n_1 = \sqrt{1 + \frac{\omega_M}{\omega_0 - \omega}}$  and  $n_2 = \sqrt{1 + \frac{\omega_M}{\omega_0 + \omega}}$ .

Obviously all of these modes in both limiting cases are characterized by ordinary refraction properties for low excitation frequencies  $\omega$ , while for large  $\omega$  one of refractive indexes becomes purely imaginary corresponding to the non-propagating regime, while other remains real and corresponds to an ordinary refraction. It should be emphasized that in the above mentioned cases with the linear polarized wave at the input always obtain linearly polarized wave at the output: In purely ferromagnetic case we find a Faraday rotation and for pure ferroelectrics just a phase shift (that however can be retrieved by interference measurements).

The situation changes drastically in the presence of both ferroelectric and ferromagnetic layers. An injected linear polarized electromagnetic wave emerges after traversing the FE/FM heterostructure with an elliptical polarization, as detailed below.

We can further simplify the analytic solutions (5) and

(6) in the general case (both ferroelectric and ferromagnetic layers are present in the system) assuming  $\alpha \rightarrow 0$  which is just the case of a large susceptibility in FE [17]. Then one infers two roots of (5). The first one matches exactly the asymptotic result (4), and the second one reads

$$n_2^2 = \frac{(\omega_0 + \omega_M)^2 - \omega^2}{\omega_0(\omega_0 + \omega_M) - \omega^2}. \quad (7)$$

Now it is evident that in the same limit of  $\alpha \rightarrow 0$ , for the first mode (4) the Poynting vector has the values  $\mathcal{W}_1 \sim -n$ , meaning that a negative refraction takes place. For the second mode (7) the Poynting vector is  $\mathcal{W}_2 \sim n$  corresponding to a positive refraction case. To identify the positive-negative birefringence regime both propagating modes should be present, i.e.  $n_1^2 > 0$  and  $n_2^2 > 0$ . From these relations we deduce the restrictions on the mode frequency

$$\text{Max}\{\omega_P, \omega_0\} < \omega < \sqrt{\omega_0(\omega_0 + \omega_M)}. \quad (8)$$

These relations set a reliable range in which positive-negative birefringence effect to be found.

## RESULTS

The exact solutions of (5) are illustrated by graphs (b) and (c) in Fig. 1. The frequency dependencies of the two roots with positive real parts  $n' > 0$  of the refractive index  $n = n' + n''$  are displayed as to pinpoint the wavevector direction and compare it with the sign of the Poynting vector as calculated according to (6). Apparently in Fig. 1 (b), the sign of the Poynting vector is negative in the frequency range close to  $\omega = 30\text{GHz}$ , i.e. the Poynting vector is antiparallel to the wave vector direction and therefore we are in the negative refraction regime, while in graph (c) another root with a positive  $n'$  is presented. The Poynting vector in this case is positive, that means we have a second mode with an ordinary (positive) refraction for the same wave frequency  $\omega = 30\text{GHz}$ . The clear evidence of the coexistence of a positive and negative refractions for an unpolarized electromagnetic wave is fully compatible with the approximate conditions (8).

To substantiate the analytical estimation we performed full numerical experiment considering two wave modes with different polarizations being injected into the FE/FM composite metastructure. An oscillating electric field with the characteristic frequency  $\omega = 30\text{GHz}$  operating on the left edge of the dipolar/spin chain is due to the action of the light source on the sample. The wave propagation proceeds self-consistently as governed by the set of equations (2) and (3). The results shown in Fig. 2 confirm evidently the existence of the birefringence effect.

In numerical simulations we act on the left end of the system with an electric field having the polarization

$\mathcal{E}_{x,y} = 0.19 + 1.81i$  and corresponding to the negative refraction regime. Obviously a Gaussian pulse propagates with a positive group velocity see Fig. 2 (a), while according to Fig. 2 (c) the phase velocity is negative (blue, green and red curves correspond to time oscillations of subsequent sites with increasing site number). Fig. 2 (b) displays the wave propagation process (again with positive group velocity) with the polarization  $\mathcal{E}_{x,y} = 0.015 + 1.985i$ . However, the corresponding phase velocity is now positive and ordinary (positive) refraction scenario holds, see Fig. 2 (d).

In the above considerations the damping effects were neglected which allows obtaining analytical expressions. In practice, ferromagnetic layers can be engineered such that the damping [20] is very small (in  $\mu\text{s}$  range) and hence can be neglected on our relevant  $ns$  time scale. In ferroelectrics damping is much stronger and its effect should be considered. FE damping impacts the first mode only (4). In the limit  $\alpha \rightarrow 0$  (i.e. for large susceptibility) the modified expression of the refraction index of the first mode reads

$$n_1^2 = \left(1 + \frac{\omega_P^2/\alpha}{\omega_P^2 - \omega^2 + i\omega\Gamma}\right) \left(1 + \frac{\omega_0\omega_M}{\omega_0^2 - \omega^2}\right), \quad (9)$$

(here  $\Gamma$  is the damping parameter) while the second mode (7) is left unchanged. The experimentally observed peaks in the susceptibility correspond to the frequency  $\omega_p = 10\text{GHz}$  see Ref [17]. In our case  $\omega = 30\text{GHz}$ ,  $\Gamma \ll \omega_P \ll \omega$ . Hence, we conclude that also FE damping has no significant effect on the first mode (9) clarifying so the role of losses for the predicted phenomena. Until now we considered FM and FE layers of equal thickness. Absorption effects are rather sensitive to the thickness of FE layers and much less sensitive to the thickness of FM layers. A recipe for minimizing losses is thus straightforward by fabricating thinner FE layers. In the numerical simulations the thickness enters through the values of  $\alpha$  in (3). For example, taking  $\alpha = 10^{-2}$  instead of  $\alpha = 10^{-4}$  in (3), one can make the average polarization 100 times smaller (which affects the electromagnetic waves). If we take the FE layer 100 times thinner than the FM layer, then the wave spends much less time in FE layer and the absorption effects are reduced drastically. On the other hand, tuning  $\alpha$  leaves the main qualitative characteristics of the considered effect unchanged.

The frequency range for which the negative refraction takes place depends on the external magnetic field (see Fig. 3). The external magnetic field induces a shift in the Larmor frequency  $\omega_0 = \omega_a + \gamma H_0$ , while the anisotropy frequency is fixed to  $\omega_a = 20\text{GHz}$ . By means of an external magnetic field the frequency  $\omega_0$  is tunable within an interval 10GHz to 50GHz. The results for the negative refraction are shown in Fig. 3 (left graph). These results confirm that the frequency range for which a negative refraction takes place can be controlled by an external magnetic field. In the experiment one may switch so neg-

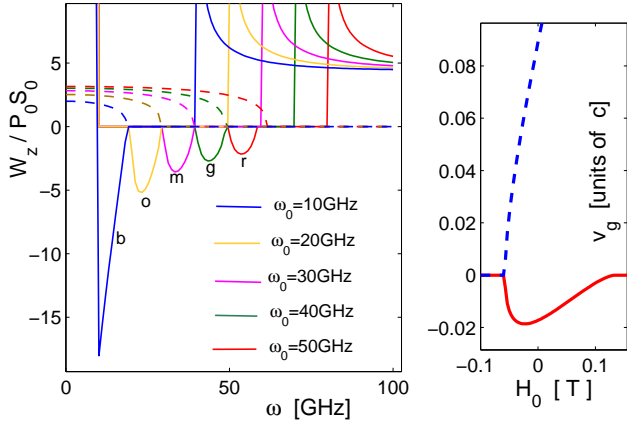


FIG. 3: Left graph: The Poynting vector magnitude versus the mode frequency for different external magnetic fields:  $\omega_0 = 10, 20, 30, 40, 50$  GHz correspond to blue (b), orange (o), magenta (m), green (g), and red (r) lines. Solid curves indicate the modes with a negative refraction regime and dashed lines describe the positively refractive ones. The frequency ranges with a vanishing Poynting vector correspond to non-propagating evanescent modes. Right graph: The mode group velocity dependence on the static magnetic field for a fixed excitation frequency  $\omega = 24$  GHz. Blue (dashed) and red (solid) curves describe the group velocities (in units of the speed of light) of positively and negatively refracting modes, respectively.

active refraction media to ordinary media and vice versa simply by turning the magnetic field off and on.

In the right graph of Fig. 3 for negatively and positively refracting waves we plot the dependence of the group velocity on a static magnetic field. It is evident that by a ramped static magnetic field we can achieve acceleration or even trapping of the electromagnetic waves. Finally we note that effects related to photonic-magneto-elastic and/or piezoelectric couplings are straightforwardly incorporated in the above formulism by including the respective energy term in eqs.(1), along the lines as done in Refs.[21, 22]. Furthermore, to access a higher frequency regime (cf. eq.7)) it would be advantages to utilize FE/aniferromagnetic/FE/.... layer structures. For example, recently an antiferromagnetic resonance frequency of 22 THz were observed for  $\text{KNiF}_3$  [23].

## SUMMARY

Summarizing, in the present work we illustrated theoretically an insulating multiferroic metamaterial featuring simultaneous positive and negative refraction (positive-negative birefringes) and provided concrete predictions for a realization on the basis of  $\text{SrTiO}_2/\text{YIG}$  multilayers. In addition to full-fledge numerical simulations for the coupled Maxwell/ferroelectric/ferromagnetic dynamics, we were

able to derive credible analytical solutions and concrete frequency regimes in which the predicted effects are to be expected. The theory and predictions are of a general nature and are applicable to a wide range of material classes. The findings point to new exciting applications of insulating nanostructured oxides in photonics.

This research is funded by the German Science foundation under SFB 762 "Functionality of Oxide Interfaces". We thank J. Schilling for comments on the experimental aspects. R. Kh. acknowledges financial support from Georgian SRNSF (grant No FR/25/6-100/14) and travel grants from Georgian SRNSF and CNR, Italy (grant No 04/24) and CNRS, France (grant No 04/01).

## APPENDIX

To obtain wave solutions of the set Eqs.(2,3) in the main text we express the field and the polarization/magnetization components as follows:

$$\begin{aligned} \mathcal{E}_m^x &= \mathcal{E}_x e^{i(\omega t - kam)} + c.c., & \mathcal{E}_m^y &= \mathcal{E}_y e^{i(\omega t - kam)} + c.c., \\ h_m^x &= h_x e^{i(\omega t - kam)} + c.c., & h_m^y &= h_y e^{i(\omega t - kam)} + c.c., \\ s_m^x &= \mathcal{S}_x e^{i(\omega t - kam)} + c.c., & s_m^y &= \mathcal{S}_y e^{i(\omega t - kam)} + c.c., \\ p_m &= \mathcal{P} e^{i(\omega t - kam)} + c.c. \end{aligned} \quad (10)$$

Substituting this into Eqs.(2,3) of the main text and considering the large wavelength limit  $k \rightarrow 0$  we find

$$\begin{aligned} i\omega(h_x + 4\pi\mathcal{S}_x) &= -ik\mathcal{E}_y, & -i\omega(h_y + 4\pi\mathcal{S}_y) &= -ik\mathcal{E}_x \\ -i\omega(\mathcal{E}_x + 4\pi\mathcal{P}) &= -ikh_y, & i\omega\mathcal{E}_y &= -ikh_x \\ i\omega\mathcal{S}_x + \omega_0\mathcal{S}_y - \frac{\omega_M}{4\pi}h_y &= 0 & i\omega\mathcal{S}_y - \omega_0\mathcal{S}_x + \frac{\omega_M}{4\pi}h_x &= 0 \\ \alpha(\omega^2 - \omega_P^2)\mathcal{P} + \frac{\omega_P^2}{4\pi}\mathcal{E}_x &= 0. \end{aligned} \quad (11)$$

After some algebra one can reduce this equation to the three coupled equations

$$\begin{aligned} i\omega(n^2 - 1)h_x + [\omega_0(n^2 - 1) - \omega_M]h_y - \omega_0n\mathcal{P} &= 0, \\ -[\omega_0(n^2 - 1) - \omega_M]h_x + i\omega(n^2 - 1)h_y - i\omega n\mathcal{P} &= 0, \\ \omega_P^2 n h_y + [\alpha(\omega^2 - \omega_P^2) - \omega_P^2]\mathcal{P} &= 0, \end{aligned} \quad (12)$$

where  $n \equiv ck/\omega$  is a refractive index. Thus finally we arrive at the matrix

$$\begin{pmatrix} i\omega(n^2 - 1) & \omega_0(n^2 - 1) - \omega_M & \omega_0 n \\ \omega_M - \omega_0(n^2 - 1) & i\omega(n^2 - 1) & -i\omega n \\ 0 & \omega_P^2 n & \alpha(\omega^2 - \omega_P^2) - \omega_P^2 \end{pmatrix}$$

the determinant of which should be equal to zero which leads to the relation

$$\begin{aligned} [(\omega^2 - \omega_P^2)\alpha - \omega_P^2] \left\{ [\omega_0(n^2 - 1) - \omega_M]^2 - \omega^2(n^2 - 1)^2 \right\} \\ + \omega_P^2 n^2 [(\omega_0^2 - \omega^2)(n^2 - 1) - \omega_M\omega_0] = 0 \end{aligned}$$

This could be straightforwardly simplified to a bi-quadratic equation for the refractive index  $n$

$$\alpha(\omega_0^2 - \omega^2)(\omega_P^2 - \omega^2)n^4 - (\omega_0^2 + \omega_M\omega_0 - \omega^2) [2\alpha(\omega_P^2 - \omega^2) + \omega_P^2]n^2 + [\alpha(\omega_P^2 - \omega^2) + \omega_P^2] [(\omega_0 + \omega_M)^2 - \omega^2] = 0$$

which is exactly the same relation (5) as in the main text.

The above matrix together with the relations (11) of this supplementary materials gives the eigenmodes of the system and defines the time averaged Poynting vector value as

$$\langle W^z \rangle = \langle E_x H_y - E_y H_x \rangle = P_0 S_0 [\mathcal{E}_x(h_y)^* - \mathcal{E}_y(h_x)^*] + c.c.$$

Defining now the dimensionless version of the Poynting vector as  $\mathcal{W} = \langle W^z \rangle / P_0 S_0$  we obtain eq.(6) of the main text

$$\mathcal{W} = n \left\{ \frac{(\omega^2 - \omega_P^2) [(\omega^2 - \omega_0^2)(n^2 - 1) + \omega_0\omega_M]}{(\omega^2 - \omega_P^2 - \omega_P^2/\alpha)\omega^2\omega_M^2} + 1 \right\}$$

which in the limit  $\alpha \rightarrow 0$  gives the following expressions for the negatively refracting  $n = n_1$  and positively refracting  $n = n_2$  modes

$$\mathcal{W}_1 = -n \frac{(\omega_0^2 + \omega_0\omega_M - \omega^2)^2\omega_P^2}{\alpha(\omega^2 - \omega_P^2)\omega^2\omega_M^2},$$

$$\mathcal{W}_2 = n \left\{ 1 - \frac{\alpha(\omega^2 - \omega_P^2)\omega^2\omega_M^2}{(\omega_0^2 + \omega_0\omega_M - \omega^2)^2\omega_P^2} \right\}$$

and as it could be easily seen  $\mathcal{W}_1 \sim -n$  for  $\omega > \omega_P$  and  $\mathcal{W}_2 \sim n$  for  $\alpha \rightarrow 0$ .

---

\* Electronic address: Jamal.Berakdar@physik.uni-halle.de

- [1] V.G. Veselago, Properties of materials having simultaneously negative values of the dielectric and magnetic susceptibilities *Sov. Phys. Solid State* **8**, 2854 (1967).
- [2] V.G. Veselago, The electrodynamics of substances with simultaneously negative values of  $\epsilon$  and  $\mu$  *Sov. Phys. Usp.* **10**, 509 (1968).
- [3] J.B. Pendry, A.J. Holden, D.J. Robbins and W. J. Stewart, Magnetism from conductors and enhanced nonlinear phenomena *IEEE Trans. Microwave Theory Tech.* **47** 2075 (1999).
- [4] D.R. Smith, W.J. Padilla, D.C. Vier, S.C. Nemat-Nasser, and S. Schultz, Composite Medium with Simultaneously Negative Permeability and Permittivity *Phys. Rev. Lett.* **84**, 4184 (2000).
- [5] R.A. Shelby, D.R. Smith and S. Schultz, Experimental Verification of a Negative Index of Refraction *Science* **292**, 7 (2001).
- [6] J. B. Pendry, Negative refraction *Contemp. Phys.* **45**, 191 (2004).
- [7] M. I. Stockman, Criterion for Negative Refraction with Low Optical Losses from a Fundamental Principle of Causality *Phys. Rev. Lett.* **98**, 177404 (2007).
- [8] D.W. Ward, K.A. Nelson, K.J. Webb, On the physical origins of the negative index of refraction *New J. Phys.* **7**, 213 (2005).
- [9] D.R. Fredkin, A. Ron, Effectively left-handed (negative index) composite material *App. Phys. Lett.* **81**, 1753 (2002).
- [10] M. Bibes and A. Barthelemy, Multiferroics: Towards a magnetoelectric memory *Nat. Mater.* **7**, 425 (2008).
- [11] D. Pantel, S. Goetze, D. Hesse, and M. Alexe, Reversible electrical switching of spin polarization in multiferroic tunnel junctions *Nat. Mater.* **11**, 289 (2012).
- [12] *Physics of Ferroelectrics*, edited by K. Rabe, Ch. H. Ahn, and J.-M. Triscone (Springer, Berlin, 2007).
- [13] A. Picinin, M.H. Lente, J.A. Eiras, and J.P. Rino, Theoretical and experimental investigations of polarization switching in ferroelectric materials *Phys. Rev. B* **69**, 064117 (2004).
- [14] J.J. Wang, P.P. Wu, X.Q. Ma, and L.Q. Chen, Temperature-pressure phase diagram and ferroelectric properties of BaTiO<sub>3</sub> single crystal based on a modified Landau potential *J. Appl. Phys.* **108**, 114105 (2010).
- [15] O.E. Fesenko and V.S. Popov, Phase T,E-diagram of barium titanate *Ferroelectrics* **37**, 729 (1981).
- [16] A. Namai, A. Namai, M. Yoshikiyo, K. Yamada, S. Sakurai, T. Goto, T. Yoshida, T. Miyazaki, M. Nakajima, T. Suemoto, H. Tokoro, and S.-i. Ohkoshi Hard magnetic ferrite with a gigantic coercivity and high frequency millimetre wave rotation *Nat. Communications*, **3**, 1035 (2012).
- [17] J. H. Haeni, P. Irvin, W. Chang, R. Uecker, P. Reiche, Y. L. Li, S. Choudhury, W. Tian, M. E. Hawley, B. Craigo, A. K. Tagantsev, X. Q. Pan, S. K. Streiffer, L. Q. Chen, S. W. Kirchoefer, J. Levy, and D. G. Schlom *et al.*, Room-temperature ferroelectricity in strained SrTiO<sub>3</sub> *Nature*, **430**, 758 (2004).
- [18] J. Xiao, G.E.W. Bauer, K.-C. Uchida, E. Saitoh, and S. Maekawa, Theory of magnon-driven spin Seebeck effect *Phys. Rev. B*, **81**, 214418 (2010).
- [19] C. Xiong, W. H. P. Pernice, J. H. Ngai, J. W. Reiner, D. Kumah, F. J. Walker, C. H. Ahn, and H. X. Tang, Active Silicon Integrated Nanophotonics: Ferroelectric BaTiO<sub>3</sub> Devices *Nano Lett.* **14**, 1419 (2014).
- [20] C. Hauser, T. Richter, N. Homonnay, Ch. Eisenschmidt, M. Qaid, H. Deniz, D. Hesse, M. Sawicki, S. G. Ebbinghaus, and G. Schmidt Yttrium Iron Garnet Thin Films with Very Low Damping Obtained by Recrystallization of Amorphous Material *Sci. Rep.*, **6** 20827 (2016).
- [21] C.-L. Jia, N. Zhang, A. Sukhov, and J. Berakdar, Ultrafast transient dynamics in composite multiferroics *New J. Phys.* **18**, 023002 (2016)
- [22] C.-L. Jia, A. Sukhov, P. P. Horley, and J. Berakdar, Piezoelectric control of the magnetic anisotropy via interface strain coupling in a composite multiferroic structure *Europhys. Lett.* **99**, 17004 (2012)
- [23] D. Bossini, S. Dal Conte, Y. Hashimoto, A. Secchi, R. V. Pisarev, Th. Rasing, G. Cerullo, and A. V. Kimel Macrospin dynamics in antiferromagnets triggered by sub-20 femtosecond injection of nanomagnons. *Nat. Commun.* **7**:10645 doi: 10.1038/ncomms10645 (2016).